Fully Tunable Longitudinal Spin-Photon Interactions in Si and Ge Quantum Dots

Stefano Bosco,[1,*] Pasquale Scarlino,[2] Jelena Klinovaja,[1] and Daniel Loss[1]

[1]*Department of Physics, University of Basel, Klingelbergstrasse 82, 4056 Basel, Switzerland*

[2]*Institute of Physics, Ecole Polytechnique Fédérale de Lausanne, CH-1015 Lausanne, Switzerland*

(Received 31 March 2022; accepted 6 July 2022; published 2 August 2022)

Spin qubits in silicon and germanium quantum dots are promising platforms for quantum computing, but entangling spin qubits over micrometer distances remains a critical challenge. Current prototypical architectures maximize transversal interactions between qubits and microwave resonators, where the spin state is flipped by nearly resonant photons. However, these interactions cause backaction on the qubit that yields unavoidable residual qubit-qubit couplings and significantly affects the gate fidelity. Strikingly, residual couplings vanish when spin-photon interactions are longitudinal and photons couple to the phase of the qubit. We show that large and tunable spin-photon interactions emerge naturally in state-of-the-art hole spin qubits and that they change from transversal to longitudinal depending on the magnetic field direction. We propose ways to electrically control and measure these interactions, as well as realistic protocols to implement fast high-fidelity two-qubit entangling gates. These protocols work also at high temperatures, paving the way toward the implementation of large-scale quantum processors.

DOI: 10.1103/PhysRevLett.129.066801

Introduction.—Spin qubits in silicon (Si) and germanium (Ge) quantum dots are frontrunner candidates to process quantum information [1–6]. Hole spin qubits hold particular promise because of their large and fully tunable spin-orbit interactions (SOIs) [7–16], enabling ultrafast all-electrical gates at low power [17–28], and because of their resilience to hyperfine noise even in natural materials [29–34]. In current quantum processors, engineering long-range interactions of distant qubits remains a critical challenge. A fast and coherent interface between qubits separated by a few micrometers will enable modular architectures with cryogenic classical control on-chip [35–39], as well as significantly improve qubit connectivity, with great advantages for near-term quantum processors [40,41] and opening up to new classes of efficient quantum error correcting codes [42–44].

Driven by significant technological progress in enhancing the amplitude of spin-photon interactions (SPIs) [45–47], coupling distant spin qubits via microwave resonators is an appealing approach [48–50]. In analogy to superconducting circuits [51–53], current SPIs are designed to be "transversal," where nearly resonant photons flip the spin state. However, these interactions cause a significant backaction of the resonator on the qubit, resulting in unavoidable residual qubit-qubit couplings. These unwanted couplings are critical issues in scalable quantum processors [54,55], and they are minimized by operating in the dispersive regime [56], where a large detuning between resonator and qubit frequencies also suppresses the effective spin-spin interactions.

In this Letter, we investigate a different approach where fast high-fidelity two-qubit gates are implemented by tunable "longitudinal" SPIs, where the photon couples to the phase of the qubit. These interactions do not cause backaction on the qubit, thus eliminating residual couplings and suppressing Purcell decay [54]. Moreover, because longitudinal interactions do not rely on resonant processes, fast two-qubit gates are possible at arbitrarily large detuning, relaxing stringent constraints imposed by dispersive interactions and frequency crowding, and helping in scaling up the next generation of quantum processors.

While challenging to engineer in superconducting circuits [54,55], large longitudinal interactions emerge naturally in hole spin qubits, where, in contrast to alternative theoretical proposals [57–63] and recent experiments [58], they do not require multiple quantum dots or parametric driving. We show that SPIs in hole dots are fully tunable as they change from transversal to longitudinal depending on the direction of the magnetic field and they are turned on and off by gate potentials. These interactions can also be harmonically modulated by ac electric fields, a mechanism that enables fast qubit readout protocols [64,65] and two-qubit gates [66,67]. We propose protocols to reliably measure and control these interactions, yielding fast entangling gates between distant qubits, with fidelities above the surface code threshold [68]. Strikingly, these gates also work at high temperatures with resonators in hot thermal states [69–71], thus providing a significant step toward large-scale universal semiconducting quantum processors.

Static spin-photon interactions.—The interactions between spins in a quantum dot and photons confined in a microwave resonator with frequency ω_r is described by the Hamiltonian

$$H = \frac{\hbar\omega_B}{2}\sigma_3 + \hbar\omega_r a^\dagger a + \hbar\boldsymbol{\gamma}\cdot\boldsymbol{\sigma}(a^\dagger + a), \tag{1}$$

where a is the photon annihilation operator and $\boldsymbol{\sigma}$ is a vector of Pauli matrices. The qubit frequency ω_B and the direction of Zeeman field $\boldsymbol{e}_3$ are related to the magnetic field $\boldsymbol{B}$ and to the matrix $\underline{g}$ of g factors by $\mu_B \boldsymbol{B}\cdot\underline{g} = \hbar\omega_B \boldsymbol{e}_3$. The SPIs are determined by the vector $\boldsymbol{\gamma}$, whose magnitude and direction strongly depends on the setup.

In long quantum dots, where the confinement potential in one direction, e.g., $\boldsymbol{e}_z$, is smoother than in the other directions, the SPIs are mediated by the SOI, and when the electric field E_r of the resonator is aligned to $\boldsymbol{e}_z$, we obtain

$$\boldsymbol{\gamma}_L = \frac{l}{l_{so}}\frac{eE_r l}{\hbar\bar{\omega}}\omega_r \boldsymbol{e}_{so} \approx \alpha\frac{l}{l_{so}}\frac{\sqrt{Z_r}}{\sqrt{\hbar\bar{\omega}}}\omega_r^2 \boldsymbol{e}_{so}. \tag{2}$$

The spin-orbit length l_{so} and the unit vector $\boldsymbol{e}_{so}$ describe the magnitude and direction of the vector of SOI, respectively; see also the Supplemental Material (SM) [72]. These parameters depend on details of the dot, including external fields, confinement potential, material growth, and strain [9–16]. We parametrize the soft and hard confinement by the harmonic length l and frequency $\bar{\omega} = \hbar/\bar{m}l^2$, and by the length L and energy $\epsilon_c = \hbar^2\pi^2/\bar{m}L^2$, respectively. We introduce the average hole mass $\bar{m} = m/\gamma_1$, where m is the bare electron mass and γ_1 is a Luttinger parameter [73]. We estimate $eE_r l \approx \alpha V_r$, where $V_r = \omega_r\sqrt{\hbar Z_r}$ is the zero-point fluctuation potential of photons at the antinode of a resonator with characteristic impedance Z_r [51–53] and α is the lever arm describing the electrostatic coupling of the plunger gate connecting the resonator to the dot.

The type of SPIs depends on the direction of $\boldsymbol{B}$. Transversal interactions are tuned into longitudinal interactions by aligning the Zeeman field to the spin-orbit vector, i.e., $\boldsymbol{e}_3 \| \boldsymbol{e}_{so}$. This field direction is generally compatible with superconducting resonators; see Fig. 1. The magnitude of $\boldsymbol{\gamma}_L$ is particularly large in hole spin qubits, where l_{so} of a few tens of nanometers, comparable to l, were measured [21,22,74], enabling strong interactions in single quantum dots [75–77].

In Fig. 1(a), we compare $\boldsymbol{\gamma}_L$ in state-of-the-art hole spin qubits encoded in Si and Ge quantum dots; see the SM [72] for more details. Importantly, the amplitude of $\boldsymbol{\gamma}_L$ is large and fully tunable by an external electric field E. By simulating long dots in Ge/Si core/shell nanowires [9,22,74,75] and in square Si finFETs [24–26], we observe that large coupling strengths $|\boldsymbol{\gamma}_L^{\mathrm{Ge}\bigcirc}|/2\pi \approx 50$ MHz and $|\boldsymbol{\gamma}_L^{\mathrm{Si}\square}|/2\pi \approx 100$ MHz are experimentally achievable at realistic fields $E \sim 10$ V/μm and for typical parameters $\alpha = 0.4e$, $\omega_r/2\pi = 5$ GHz, and $Z_r = 4$ kΩ (yielding $V_r = 20$ μV) [79]. At small E, similar values of $|\boldsymbol{\gamma}_L|$ emerge in triangular Si finFETs [23,80–82], where the lower symmetry of the cross section permits one to completely turn off the SOI at finite values of E [11] (marked with a triangle). We also examine a quantum dot in strained planar Ge/SiGe heterostructures, an architecture that holds much promise for scaling up quantum computers [18–20]. Squeezing the dot, such that the harmonic lengths defining the dot are w and l, and satisfy $w \ll l$, induces a large SOI [13], and enables significant SPIs, with $|\boldsymbol{\gamma}_L^{\mathrm{pGe}}|/2\pi \approx 20$ MHz.

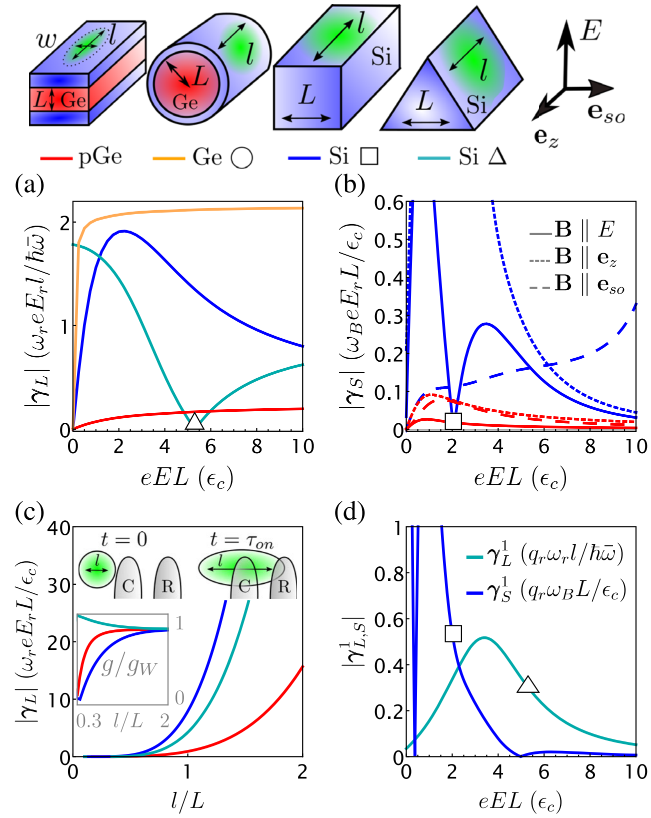

FIG. 1. Top: the devices analyzed and the color code used. Bottom: interactions of hole spin qubits and microwave photons. The magnitude of the static interactions (a) $\boldsymbol{\gamma}_L$ and (b) $\boldsymbol{\gamma}_S$ against E. In state-of-the-art architectures, $\boldsymbol{\gamma}/2\pi \sim 100$ MHz, and E is in the V/μm range, enabling strong SPI. (c) By modulating l in a time τ_{on}, $\boldsymbol{\gamma}_L$ can turn on and off. A control gate C tunes l and, in the off state, screens the gate R connected to the resonator. Inset: variation of the g factor during the protocol. In Si and Ge, $eEL = 3\epsilon_c$ and $eEL = 5\epsilon_c$, respectively, and $g_W^{\mathrm{pGe}} = 0.27$, $g_W^{\mathrm{Si}\square} = 1.15$, and $g_W^{\mathrm{Si}\Delta} = 2.8$. (d) Harmonically modulated interactions $\boldsymbol{\gamma}_{L,S}^1$. Squares and triangles indicate $\boldsymbol{\gamma}^0 = 0$, $q_r = e^2 E_r L/\epsilon_c$, and $\epsilon_c = \hbar^2\pi^2/\bar{m}L^2$. The Ge qubits are encoded in squeezed dots [13] in Ge/SiGe heterostructures with $L = 30$ nm, $l = 5w = 50$ nm, and strain energy $\epsilon_s = 15$ meV [78], and in Ge/Si core/shell nanowires with $l = 5L = 25$ nm and $\epsilon_s = 25$ meV [16]. The Si qubits are encoded in square and triangular fin field-effect transistors (FETs) with $l = 2L = 20$ nm. We consider isotropic Ge [73], and in Si we use the growth direction $\boldsymbol{e}_z \|[001]$, $E\|[110]$, where SOIs are maximal [10] (fully tunable [11,29]) in square (triangular) FETs.

These interactions are enhanced by modifying the quantum dot, e.g., using lightly strained materials and tightly squeezed dots [13], or by increasing the resonators impedance, either in superconducting platforms [83–86] or in carbon nanotubes [87–89] and quantum Hall materials [61,67,90,91], where $Z_r \approx 25$ kΩ. Also, importantly, $\boldsymbol{\gamma}_L$ is independent of the amplitude of $\boldsymbol{B}$, but depends quadratically on ω_r; see Eq. (2): increasing ω_r has a large effect on the interactions, enabling $|\boldsymbol{\gamma}_L|/2\pi \sim 1$ GHz at $\omega_r/2\pi = 20$ GHz. As longitudinal interactions do not require ω_r and ω_B to be matched [66], it is convenient to couple high-frequency resonators, e.g., $\omega_r/2\pi \sim 20$ GHz, with low frequency qubits, e.g., $\omega_B/2\pi \sim 1$ GHz, that work at small values of $|\boldsymbol{B}|$, and are thus compatible with superconducting cavities. This regime also suppresses unwanted residual transversal interactions that affect scalability [54,55]. For example, when $\boldsymbol{B}$ is misaligned by $\eta = 1\%$ from $\boldsymbol{e}_{so}$, the residual transversal interactions are dispersive, i.e., $\chi a^\dagger a \sigma_z$ [51–53], and have negligible amplitude $\chi \approx \eta^2 |\boldsymbol{\gamma}_L|^2/(\omega_r - \omega_B) \lesssim 10^{-5}|\boldsymbol{\gamma}_L|$.

In hole spin qubits, large SPIs arise also from the electrical tunability of the Zeeman energy [22]. When $\boldsymbol{B}$ is misaligned to a principal axis i of the g factor (defined by $\underline{g} = \delta_{ij} g_i$), this tunability yields fast spin flips [92–96] and transversal interactions, while when $\boldsymbol{B} \| \boldsymbol{e}_i$ the interactions are longitudinal. In the architectures examined, $\boldsymbol{e}_i$ coincide with the main confinement axis [97] and a resonator field $E_r \| E$ yields

$$\boldsymbol{\gamma}_S = \frac{\mu_B}{2\hbar} \frac{\partial \underline{g} \cdot \boldsymbol{B}}{\partial E} E_r \approx \frac{\alpha}{2 e l g_i} \frac{\partial g_i}{\partial E} \sqrt{\hbar Z_r} \omega_r \omega_B \boldsymbol{e}_3. \quad (3)$$

In Fig. 1(b), we compare $\boldsymbol{\gamma}_S$ in Si finFETs and in planar Ge for different directions of $\boldsymbol{B}$. We assume that ω_B is constant and variations of g_i at different E are compensated by $\boldsymbol{B}$. Importantly, this interaction is turned off at the sweet spots with $\partial g_i/\partial E = 0$, where charge noise is suppressed to first order (marked with a square). Because of the anisotropy of the g factor, the presence of these sweet spots depends on the direction of $\boldsymbol{B}$; we find similar trends and sweet spots also in the other architectures examined [11,16,29]. In contrast to $\boldsymbol{\gamma}_L$, here $\boldsymbol{\gamma}_S \propto \omega_B \omega_r$, resulting in a lower enhancement of the longitudinal interactions by operating at $\omega_B \ll \omega_r$. Working in this regime, however, still suppresses residual dispersive interactions arising, e.g., from small misalignments of $\boldsymbol{B}$ from $\boldsymbol{e}_i$. We emphasize that, while typically smaller than $\boldsymbol{\gamma}_L$, $\boldsymbol{\gamma}_S$ conveniently results in significant interactions also in short quantum dots.

Tuning the interactions.—The SPIs are fully tunable and by changing electric potentials, they can be turned on and off on demand. To tune $\boldsymbol{\gamma}_L$, we consider the protocol sketched in Fig. 1(c), where a gate (C) controls the length l and the position of the dot. In the off state, the dot is short and C screens the electric field of the gate (R) connected to the resonator, suppressing $\boldsymbol{\gamma}_L$. By elongating the dot, the interactions are turned on and $\boldsymbol{\gamma}_L$ is enhanced by orders of magnitude because $\boldsymbol{\gamma}_L \propto l^4$ [see Eq. (2)] and E_r is not screened by C. Adiabatically switching on $\boldsymbol{\gamma}_L$ in a time $\tau_{\rm on} \lesssim \omega_B/2\pi$ reduces errors and leakage during this protocol. We emphasize that, as shown in the inset of Fig. 1(c), the g factor also changes [13,16] during the protocol, yielding an additional phase accumulation in the qubit that can be compensated for by single-qubit gates or by appropriately modifying $\boldsymbol{B}$.

Moreover, we analyze the possibility to harmonically modulate the interactions, i.e., $\boldsymbol{\gamma} \to \boldsymbol{\gamma}\cos(\omega t)$. This type of SPI enables efficient qubit readout [64] and two-qubit gates [66,67]. Because in current experiments the size of the dot is varied in $\tau_{\rm on} \sim 1$ ns [98–100], the protocol in Fig. 1(c) could be adapted to harmonically modulate $\boldsymbol{\gamma}_L$. However, the strong nonlinear dependence of $\boldsymbol{\gamma}_L$ on l might significantly distort the ac signal. To reduce distortion, we propose instead to superimpose a small ac field $\delta E\cos(\omega t)$ to the dc field E, yielding the parametrically modulated interactions

$$\boldsymbol{\gamma}(t) \cdot \boldsymbol{\sigma}(a^\dagger + a) \approx [\boldsymbol{\gamma}^0 + \boldsymbol{\gamma}^1 \delta E \cos(\omega t)] \cdot \boldsymbol{\sigma}(a^\dagger + a). \quad (4)$$

The dependence of $\boldsymbol{\gamma}^1_{L,S}$ on E in Si finFETs is shown in Fig. 1(d). The sweet spots where $\boldsymbol{\gamma}_0 = 0$ (squares and triangles) are particularly relevant because there the static interactions are off when $\delta E = 0$, and the qubit lifetime is enhanced by the lower susceptibility to charge noise. By using $\delta E = 0.1$ V/μm, $\omega_r/2\pi = \omega_B/2\pi = 5$ GHz, $V_r = 20$ μV, and $\alpha = 0.4e$, we estimate that at the sweet spots $\boldsymbol{\gamma}^1_L \delta E/2\pi \sim 10 \boldsymbol{\gamma}^1_S \delta E/2\pi \approx 0.5$ MHz is comparable to current experiments [58] and is significantly enhanced by enlarging ω_r, yielding $\boldsymbol{\gamma}^1_L \delta E/2\pi \approx 10$ MHz at $\omega_r/2\pi \approx 25$ GHz. However, far from the sweet spots, $\boldsymbol{\gamma}^1$ is much smaller than $\boldsymbol{\gamma}^0$. For this reason, we now discuss ways to detect and use static longitudinal interactions.

Signatures of longitudinal interactions.—In contrast to transversal SPIs, longitudinal SPIs do not induce spin flips or qubit-dependent shifts of ω_r [51–53,101], and thus characterizing them is a challenging task. While ac-modulated longitudinal interactions yield a measurable asymmetry of the qubit energy against the detuning [58], this approach fails to measure static interactions. We propose instead an alternative protocol based on the backaction of longitudinal interactions on externally driven spin rotations. This protocol is not unique of hole spin qubits and works in any system described by Eq. (1).

We consider an external driving of the qubit with frequency ω_x and amplitude λ_x, inducing Rabi oscillations. By preparing the resonator in the coherent state $|\sqrt{\bar{n}} e^{i\omega_z t}\rangle$ with $\bar{n}$ photons, Eq. (1) at $\boldsymbol{\gamma} \| \boldsymbol{e}_3$ yields

$$H_M = \frac{\hbar\omega_B}{2}\sigma_3 + \hbar\lambda_x \cos(\omega_x t)\sigma_1 + \hbar\lambda_z \cos(\omega_z t + \phi)\sigma_3, \quad (5)$$

with $\lambda_z = 2\sqrt{\bar{n}}|\boldsymbol{\gamma}|$ and a phase difference ϕ.

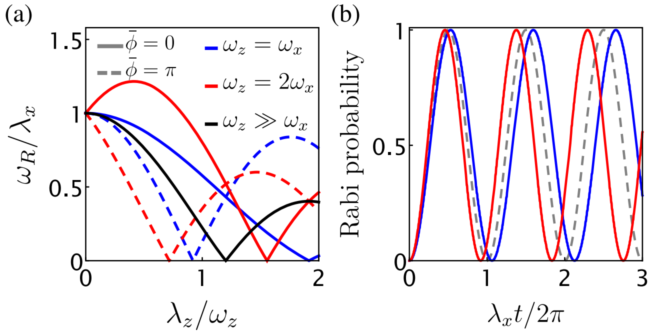

FIG. 2. Signatures of longitudinal interactions in ω_R. (a) The Rabi frequency ω_R against λ_z. We fix $\omega_B=\omega_x$ and vary ω_z and the phase $\bar{\phi}=2\omega_x(\phi+\pi)/\omega_z$. (b) The spin-flip probability in time, computed numerically from H_M in Eq. (5). Here, $\omega_x=5\lambda_z=50\lambda_x$, $\bar{\phi}=0$, and $\omega_z/\omega_x=1(2)$ for the blue (red) line. A dashed line refers to the oscillations at $\lambda_z=0$.

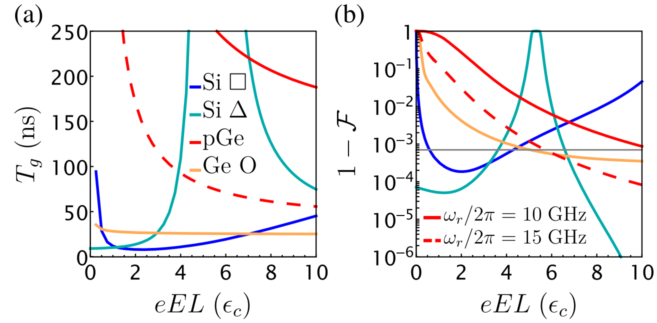

FIG. 3. Controlled-Z gate of distant qubits. We show the gate time T_g in (a) and the infidelity $1-\mathcal{F}$ (in logarithmic scale) in (b) against E. We analyze the qubits described in Fig. 1 (using the same color code), and resonators with $\alpha=0.3e$, $Z_r=4$ kΩ, and we mark with solid (dashed) lines the case $\omega_r/2\pi=10(15)$ GHz. The gray line indicates the surface code threshold $1-\mathcal{F}=7\times10^{-4}$ [68]. We consider $\omega_B/2\pi=5$ GHz and $1/f$ charge noise with $\alpha\bar{V}/\epsilon_c=0.2\times10^{-3}$.

At resonance $\omega_B=\omega_x$, and at $\lambda_z=0$, the state of the qubit rotates with Rabi frequency $\omega_R/2\pi=\lambda_x/2\pi\sim$ 50–500 MHz [18–23]. Finite values of λ_z significantly alter the speed of spin precession. By moving to the rotating frame with the operator $e^{-i\sigma_z[\omega_x t/2+\lambda_z\sin(\omega_z t+\phi)/\omega_z]}$, that accounts *exactly* for λ_z, and in the rotating wave approximation, we find [72]

$$\omega_R=\lambda_x J_0\left(\frac{2\lambda_z}{\omega_z}\right)=\lambda_x\left[1-\frac{\lambda_z^2}{\omega_z^2}+\mathcal{O}\left(\frac{\lambda_z^4}{\omega_z^4}\right)\right],\qquad(6)$$

with J_0 being the Bessel function. The correction is quadratic in λ_z/ω_z but is still detectable in current architectures. For realistic parameters $|\gamma|/2\pi=100$ MHz, $\omega_z/2\pi=5$ GHz, and in cavities with $\bar{n}=100$ photons, ω_R shifts by $\sim$15% from λ_x.

Surprisingly, Eq. (6) is valid for arbitrary values of λ_z and ω_z; however, strikingly, at certain resonant frequencies $\omega_x=q\omega_z$, with $q=1/2$ or $q\in\mathbb{N}$, the longitudinal corrections are modified by an extra phase-dependent term and read

$$\omega_R^q=\lambda_x\left|J_0\left(\frac{2\lambda_z}{\omega_z}\right)+e^{2iq(\phi+\pi)}J_{2q}\left(\frac{2\lambda_z}{\omega_z}\right)\right|.\qquad(7)$$

A detailed analysis of these resonances is provided in the SM [72]. In Fig. 2, we also confirm the shift of ω_R by numerically solving the Schrödinger equation with the Hamiltonian H_M from Eq. (5). For weak driving $\lambda_z\lesssim\omega_z$, the sensitivity of ω_R on λ_z is strongly enhanced at $q=1/2$ ($\omega_z=2\omega_x$), where $\omega_R^{q=1/2}/\lambda_x\approx1-\cos(\phi)\lambda_z/\omega_z$, is *linearly* dependent on λ_z/ω_z. Doubling $\omega_z\approx\omega_r$ enhances $\lambda_z/\omega_z\propto\omega_z$ [see Eq. (2)], yielding a maximal change of ω_R of $\sim$90% for the same parameters used above. Interestingly, at $\omega_z=2\omega_x$ and $\phi=\pi$, λ_z enhances ω_R up to 22%.

High-fidelity two-qubit gates.—When two qubits are longitudinally coupled with magnitude $\gamma_{1,2}$ to the same resonator with frequency ω_r, the resonator mediates effective Ising interactions $-J\sigma_z^1\sigma_z^2$, with exchange $J=2\gamma_1\gamma_2/\omega_r$ [54]. A controlled-Z gate between these qubits $U_{\rm cZ}=\mathrm{diag}(1,1,1,-1)\cong e^{i\pi\sigma_z^1\sigma_z^2/4}$ is implemented by switching on J for a time $T_g=\pi/4J$ ($\cong$ indicates equivalence up to single-qubit gates) [72,102]. We consider two identical qubits encoded in the realistic systems discussed above. The large value of γ results in fast gates with $T_g\sim$ 10–100 ns [see Fig. 3(a)], comparable to current superconducting qubits [103,104]. Also, T_g is significantly shortened at large ω_r because $J\propto\omega_r^3$.

Our approach relies on the ability to turn γ on and off, as sketched in Fig. 1(c), and does not require harmonically modulated interactions [62,66,67]. More precisely, when γ is abruptly switched on for a time T_g, the system evolves according to the *exact* unitary transformation up to single-qubit operations

$$U=e^{i(\pi/4)\{1-[\sin(x)/x]\}\sigma_z^1\sigma_z^2}e^{(\gamma/\omega_r)(1-e^{-ix})(\sigma_z^1+\sigma_z^2)(a-a^\dagger)}e^{-ixa^\dagger a},\qquad(8)$$

which coincides with $U_{\rm cZ}$ when $x=\omega_r T_g=2\pi n$ with $n\in\mathbb{N}$ [66]; an analogous exact solution valid for smooth pulses is presented in the SM [72]. Strikingly, in this case *arbitrary* initial states of the resonator, including hot thermal states, are unaltered after the operation, yielding no residual backaction on the qubit and suggesting that fast two-qubit gates could be executed at high temperatures. Demonstrating entangling gates at 4 K, compatible to single-qubit gates [23] and cryo-CMOS [35–39], will pave the way toward large-scale quantum computers.

Gates mediated by longitudinal interactions also have high fidelity. To examine the fidelity $\mathcal{F}$, we consider that errors can arise from the decay rate $\kappa\approx n_{\rm th}\omega_r/Q$ [105] of photons in resonators with quality factor Q and thermal population $n_{\rm th} = (e^{\hbar\omega_r/k_B T} - 1)^{-1}$. This noise channel yields a resonator-dependent dephasing of the qubits with time $T_r \approx \omega_r^2/\gamma^2\kappa \approx T_g Q/n_{\rm th}$ [66,67]. However, in state-of-the-art resonators with $Q \sim 10^4$–10^5 [79], we estimate $T_r \gtrsim 0.1/n_{\rm th}$ ms, much larger than the dephasing time of current hole spin qubits $T_2^\varphi \sim 0.1$–$10\ \mu$s when $n_{\rm th} \lesssim 10$, corresponding to $T \approx 5$ K at $\omega_r/2\pi = 10$ GHz. Moreover, residual transversal interactions caused by small misalignments of $\boldsymbol{B}$ from $\boldsymbol{e}_{so}$ with angle η yield infidelities $1 - \mathcal{F} \approx 0.8(1+\bar{n})\eta^2 \sim 10^{-3}$–$10^{-4}$ (see the SM [72]) at $\eta \approx 1\%$ and for resonators with up to $\bar{n} = 10$ photons. This infidelity is suppressed by accurately aligning $\boldsymbol{B}$, so we focus now on the intrinsic qubit noise, resulting in

$$\mathcal{F} = e^{-(T_g/T_2^\varphi)^2}, \quad \text{with} \quad \frac{1}{T_2^\varphi} = \frac{\omega_B}{2g\sqrt{\pi}}\bar{V}\frac{\partial g}{\partial V}\sqrt{\ln\left(\frac{1}{\omega_{co}T_g}\right)}, \tag{9}$$

where $\omega_{co} \approx 1$ Hz is a frequency cutoff. The gate infidelity $1 - \mathcal{F}$ in different architectures is shown in Fig. 3(b). We consider dephasing caused by a $1/f$ charge noise [106–108] with spectral function $S(\omega) = \bar{V}^2/|\omega|$ arising from random fluctuations of the gate potential. Assuming that the control gate causes the largest fluctuations, we estimate $\partial g/\partial V \approx \alpha\partial g/eL\partial E$, where typical values of $\alpha\bar{V} \sim 0.1$–$10\ \mu$eV [3,109] yield realistic T_2^φ in the μs range. In state-of-the-art devices we estimate high fidelities with $1 - \mathcal{F} \sim 10^{-3}$–$10^{-4}$, above the surface code threshold [68], and pushing long-distance coupling to new speed and coherence standards.

Conclusion.—We analyze longitudinal SPIs in Si and Ge hole quantum dots. We show that these interactions are large, fully tunable, and can be harmonically modulated. We propose protocols to quantify these interactions and to perform fast high-fidelity two-qubit gates that also work at high temperature. Engineering large longitudinal interactions in hole spin qubits will provide a significant step toward the implementation of a large-scale semiconductor quantum computer.

We thank L. Camenzind, S. Geyer, T. Patlatiuk, and A. Kuhlmann for useful discussions. This work was supported as a part of NCCR SPIN funded by the Swiss National Science Foundation (grant no. 51NF40-180604).

*Corresponding author.
stefano.bosco@unibas.ch

[1] G. Scappucci, C. Kloeffel, F. A. Zwanenburg, D. Loss, M. Myronov, J.-J. Zhang, S. De Franceschi, G. Katsaros, and M. Veldhorst, The germanium quantum information route, Nat. Rev. Mater. **6**, 926 (2021).

[2] C. Kloeffel and D. Loss, Prospects for spin-based quantum computing in quantum dots, Annu. Rev. Condens. Matter Phys. **4**, 51 (2013).

[3] G. Burkard, T. D. Ladd, J. M. Nichol, A. Pan, and J. R. Petta, Semiconductor spin qubits, arXiv:2112.08863.

[4] A. M. J. Zwerver *et al.*, Qubits made by advanced semiconductor manufacturing, Nat. Electron **5**, 184 (2022).

[5] A. Mills, C. Guinn, M. Gullans, A. Sigillito, M. Feldman, E. Nielsen, and J. Petta, Two-qubit silicon quantum processor with operation fidelity exceeding 99%, arXiv: 2111.11937.

[6] D. Jirovec, A. Hofmann, A. Ballabio, P. M. Mutter, G. Tavani, M. Botifoll, A. Crippa, J. Kukucka, O. Sagi, F. Martins, J. Saez-Mollejo, I. Prieto, M. Borovkov, J. Arbiol, D. Chrastina, G. Isella, and G. Katsaros, A singlet-triplet hole spin qubit in planar Ge, Nat. Mater. **20**, 1106 (2021).

[7] D. V. Bulaev and D. Loss, Electric Dipole Spin Resonance for Heavy Holes in Quantum Dots, Phys. Rev. Lett. **98**, 097202 (2007).

[8] D. V. Bulaev and D. Loss, Spin Relaxation and Decoherence of Holes in Quantum Dots, Phys. Rev. Lett. **95**, 076805 (2005).

[9] C. Kloeffel, M. Trif, and D. Loss, Strong spin-orbit interaction and helical hole states in Ge/Si nanowires, Phys. Rev. B **84**, 195314 (2011).

[10] C. Kloeffel, M. J. Rančić, and D. Loss, Direct Rashba spin-orbit interaction in Si and Ge nanowires with different growth directions, Phys. Rev. B **97**, 235422 (2018).

[11] S. Bosco, B. Hetényi, and D. Loss, Hole spin qubits in Si finfets with fully tunable spin-orbit coupling and sweet spots for charge noise, PRX Quantum **2**, 010348 (2021).

[12] B. Venitucci and Y.-M. Niquet, Simple model for electrical hole spin manipulation in semiconductor quantum dots: Impact of dot material and orientation, Phys. Rev. B **99**, 115317 (2019).

[13] S. Bosco, M. Benito, C. Adelsberger, and D. Loss, Squeezed hole spin qubits in Ge quantum dots with ultrafast gates at low power, Phys. Rev. B **104**, 115425 (2021).

[14] L. A. Terrazos, E. Marcellina, Z. Wang, S. N. Coppersmith, M. Friesen, A. R. Hamilton, X. Hu, B. Koiller, A. L. Saraiva, D. Culcer, and R. B. Capaz, Theory of hole-spin qubits in strained germanium quantum dots, Phys. Rev. B **103**, 125201 (2021).

[15] Z. Wang, E. Marcellina, A. R. Hamilton, J. H. Cullen, S. Rogge, J. Salfi, and D. Culcer, Optimal operation points for ultrafast, highly coherent Ge hole spin-orbit qubits, npj Quantum Inf. **7**, 54 (2021).

[16] C. Adelsberger, M. Benito, S. Bosco, J. Klinovaja, and D. Loss, Hole-spin qubits in Ge nanowire quantum dots: Interplay of orbital magnetic field, strain, and growth direction, Phys. Rev. B **105**, 075308 (2022).

[17] H. Watzinger, J. Kukučka, L. Vukušić, F. Gao, T. Wang, F. Schäffler, J.-J. Zhang, and G. Katsaros, A germanium hole spin qubit, Nat. Commun. **9**, 3902 (2018).

[18] N. W. Hendrickx, W. I. L. Lawrie, L. Petit, A. Sammak, G. Scappucci, and M. Veldhorst, A single-hole spin qubit, Nat. Commun. **11**, 3478 (2020).

[19] N. Hendrickx, D. Franke, A. Sammak, G. Scappucci, and M. Veldhorst, Fast two-qubit logic with holes in germanium, Nature (London) **577**, 487 (2020).

[20] N. W. Hendrickx, W. I. L. Lawrie, M. Russ, F. van Riggelen, S. L. de Snoo, R. N. Schouten, A. Sammak, G. Scappucci, and M. Veldhorst, A four-qubit germanium quantum processor, Nature (London) **591**, 580 (2021).

[21] K. Wang, G. Xu, F. Gao, H. Liu, R.-L. Ma, X. Zhang, Z. Wang, G. Cao, T. Wang, J.-J. Zhang, D. Culcer, X. Hu, H.-W. Jiang, H.-O. Li, G.-C. Guo, and G.-P. Guo, Ultrafast coherent control of a hole spin qubit in a germanium quantum dot, Nat. Commun. **13**, 206 (2022).

[22] F. N. M. Froning, L. C. Camenzind, O. A. H. van der Molen, A. Li, E. P. A. M. Bakkers, D. M. Zumbühl, and F. R. Braakman, Ultrafast hole spin qubit with gate-tunable spin–orbit switch functionality, Nat. Nanotechnol. **16**, 308 (2021).

[23] L. C. Camenzind, S. Geyer, A. Fuhrer, R. J. Warburton, D. M. Zumbühl, and A. V. Kuhlmann, A hole spin qubit in a fin field-effect transistor above 4 kelvin, Nat. Electron. **5**, 178 (2022).

[24] R. Maurand, X. Jehl, D. Kotekar-Patil, A. Corna, H. Bohuslavskyi, R. Laviéville, L. Hutin, S. Barraud, M. Vinet, M. Sanquer, and S. De Franceschi, A CMOS silicon spin qubit, Nat. Commun. **7**, 13575 (2016).

[25] B. Voisin, R. Maurand, S. Barraud, M. Vinet, X. Jehl, M. Sanquer, J. Renard, and S. De Franceschi, Electrical control of g-factor in a few-hole silicon nanowire mosfet, Nano Lett. **16**, 88 (2016).

[26] N. Piot, B. Brun, V. Schmitt, S. Zihlmann, V. Michal, A. Apra, J. Abadillo-Uriel, X. Jehl, B. Bertrand, H. Niebojewski, L. Hutin, M. Vinet, M. Urdampilleta, T. Meunier, Y.-M. Niquet, R. Maurand, and S. De Franceschi, A single hole spin with enhanced coherence in natural silicon, arXiv:2201.08637.

[27] E. I. Rashba, Theory of electric dipole spin resonance in quantum dots: Mean field theory with Gaussian fluctuations and beyond, Phys. Rev. B **78**, 195302 (2008).

[28] V. N. Golovach, M. Borhani, and D. Loss, Electric-dipole-induced spin resonance in quantum dots, Phys. Rev. B **74**, 165319 (2006).

[29] S. Bosco and D. Loss, Fully Tunable Hyperfine Interactions of Hole Spin Qubits in Si and Ge Quantum Dots, Phys. Rev. Lett. **127**, 190501 (2021).

[30] J. Fischer and D. Loss, Hybridization and Spin Decoherence in Heavy-Hole Quantum Dots, Phys. Rev. Lett. **105**, 266603 (2010).

[31] J. Fischer, W. A. Coish, D. V. Bulaev, and D. Loss, Spin decoherence of a heavy hole coupled to nuclear spins in a quantum dot, Phys. Rev. B **78**, 155329 (2008).

[32] J. H. Prechtel, A. V. Kuhlmann, J. Houel, A. Ludwig, S. R. Valentin, A. D. Wieck, and R. J. Warburton, Decoupling a hole spin qubit from the nuclear spins, Nat. Mater. **15**, 981 (2016).

[33] R. J. Warburton, Single spins in self-assembled quantum dots, Nat. Mater. **12**, 483 (2013).

[34] P. Philippopoulos, S. Chesi, and W. A. Coish, First-principles hyperfine tensors for electrons and holes in gaas and silicon, Phys. Rev. B **101**, 115302 (2020).

[35] L. M. K. Vandersypen, H. Bluhm, J. S. Clarke, A. S. Dzurak, R. Ishihara, A. Morello, D. J. Reilly, L. R. Schreiber, and M. Veldhorst, Interfacing spin qubits in quantum dots and donors—hot, dense, and coherent, npj Quantum Inf. **3**, 34 (2017).

[36] M. F. Gonzalez-Zalba, S. de Franceschi, E. Charbon, T. Meunier, M. Vinet, and A. S. Dzurak, Scaling silicon-based quantum computing using CMOS technology, Nat. Electron. **4**, 872 (2021).

[37] X. Xue *et al.*, CMOS-based cryogenic control of silicon quantum circuits, Nature (London) **593**, 205 (2021).

[38] J. M. Boter, J. P. Dehollain, J. P. G. van Dijk, T. Hensgens, R. Versluis, J. S. Clarke, M. Veldhorst, F. Sebastiano, and L. M. K. Vandersypen, A sparse spin qubit array with integrated control electronics, in *2019 IEEE International Electron Devices Meeting (IEDM)* (IEEE, San Francisco, CA, 2019), pp. 31.4.1–31.4.4., 10.1109/IEDM19573.2019.8993570.

[39] J. M. Boter, J. P. Dehollain, J. P. van Dijk, Y. Xu, T. Hensgens, R. Versluis, H. W. Naus, J. S. Clarke, M. Veldhorst, F. Sebastiano, and L. M. K. Vandersypen, The spider-web array–a sparse spin qubit array, arXiv:2110.00189.

[40] N. M. Linke, D. Maslov, M. Roetteler, S. Debnath, C. Figgatt, K. A. Landsman, K. Wright, and C. Monroe, Experimental comparison of two quantum computing architectures, Proc. Natl. Acad. Sci. U.S.A. **114**, 3305 (2017).

[41] A. Holmes, S. Johri, G. G. Guerreschi, J. S. Clarke, and A. Y. Matsuura, Impact of qubit connectivity on quantum algorithm performance, Quantum Sci. Technol. **5**, 025009 (2020).

[42] N. P. Breuckmann and J. N. Eberhardt, Quantum low-density parity-check codes, PRX Quantum **2**, 040101 (2021).

[43] D. Gottesman, Fault-tolerant quantum computation with constant overhead, Quantum Inf. Comput. **14**, 1338 (2014).

[44] L. Z. Cohen, I. H. Kim, S. D. Bartlett, and B. J. Brown, Low-overhead fault-tolerant quantum computing using long-range connectivity, Sci. Adv. **8**, eabn1717 (2022).

[45] A. J. Landig, J. V. Koski, P. Scarlino, U. C. Mendes, A. Blais, C. Reichl, W. Wegscheider, A. Wallraff, K. Ensslin, and T. Ihn, Coherent spin–photon coupling using a resonant exchange qubit, Nature (London) **560**, 179 (2018).

[46] X. Mi, M. Benito, S. Putz, D. M. Zajac, J. M. Taylor, G. Burkard, and J. R. Petta, A coherent spin–photon interface in silicon, Nature (London) **555**, 599 (2018).

[47] J. J. Viennot, M. C. Dartiailh, A. Cottet, and T. Kontos, Coherent coupling of a single spin to microwave cavity photons, Science **349**, 408 (2015).

[48] P. Harvey-Collard, J. Dijkema, G. Zheng, A. Sammak, G. Scappucci, and L. M. K. Vandersypen, Coherent Spin-Spin Coupling Mediated by Virtual Microwave Photons, Phys. Rev. X **12**, 021026 (2022).

[49] M. Benito, J. R. Petta, and G. Burkard, Optimized cavity-mediated dispersive two-qubit gates between spin qubits, Phys. Rev. B **100**, 081412(R) (2019).

[50] A. Warren, E. Barnes, and S. E. Economou, Long-distance entangling gates between quantum dot spins mediated by a superconducting resonator, Phys. Rev. B **100**, 161303(R) (2019).

[51] A. Blais, A. L. Grimsmo, S. M. Girvin, and A. Wallraff, Circuit quantum electrodynamics, Rev. Mod. Phys. **93**, 025005 (2021).

[52] A. Blais, R.-S. Huang, A. Wallraff, S. M. Girvin, and R. J. Schoelkopf, Cavity quantum electrodynamics for superconducting electrical circuits: An architecture for quantum computation, Phys. Rev. A **69**, 062320 (2004).

[53] A. Blais, J. Gambetta, A. Wallraff, D. I. Schuster, S. M. Girvin, M. H. Devoret, and R. J. Schoelkopf, Quantum-information processing with circuit quantum electrodynamics, Phys. Rev. A **75**, 032329 (2007).

[54] P.-M. Billangeon, J. S. Tsai, and Y. Nakamura, Circuit-QED-based scalable architectures for quantum information processing with superconducting qubits, Phys. Rev. B **91**, 094517 (2015).

[55] S. Richer and D. DiVincenzo, Circuit design implementing longitudinal coupling: A scalable scheme for superconducting qubits, Phys. Rev. B **93**, 134501 (2016).

[56] M. Boissonneault, J. M. Gambetta, and A. Blais, Dispersive regime of circuit QED: Photon-dependent qubit dephasing and relaxation rates, Phys. Rev. A **79**, 013819 (2009).

[57] P.-Q. Jin, M. Marthaler, A. Shnirman, and G. Schön, Strong Coupling of Spin Qubits to a Transmission Line Resonator, Phys. Rev. Lett. **108**, 190506 (2012).

[58] C. Bøttcher, S. Harvey, S. Fallahi, G. Gardner, M. Manfra, U. Vool, S. Bartlett, and A. Yacoby, Parametric longitudinal coupling between a high-impedance superconducting resonator and a semiconductor quantum dot singlet-triplet spin qubit, arXiv:2107.10269.

[59] S. P. Harvey, C. G. L. Bøttcher, L. A. Orona, S. D. Bartlett, A. C. Doherty, and A. Yacoby, Coupling two spin qubits with a high-impedance resonator, Phys. Rev. B **97**, 235409 (2018).

[60] F. Beaudoin, D. Lachance-Quirion, W. A. Coish, and M. Pioro-Ladrière, Coupling a single electron spin to a microwave resonator: Controlling transverse and longitudinal couplings, Nanotechnology **27**, 464003 (2016).

[61] S. Bosco and D. P. DiVincenzo, Transmission lines and resonators based on quantum hall plasmonics: Electromagnetic field, attenuation, and coupling to qubits, Phys. Rev. B **100**, 035416 (2019).

[62] R. Ruskov and C. Tahan, Modulated longitudinal gates on encoded spin qubits via curvature couplings to a superconducting cavity, Phys. Rev. B **103**, 035301 (2021).

[63] X.-Y. Zhu, T. Tu, A.-L. Guo, Z.-q. Zhou, C.-F. Li, and G.-C. Guo, Dynamics of probing a quantum-dot spin qubit with superconducting resonator photons, Sci. Rep. **8**, 15761 (2018).

[64] N. Didier, J. Bourassa, and A. Blais, Fast Quantum Nondemolition Readout by Parametric Modulation of Longitudinal Qubit-Oscillator Interaction, Phys. Rev. Lett. **115**, 203601 (2015).

[65] R. Ruskov and C. Tahan, Quantum-limited measurement of spin qubits via curvature couplings to a cavity, Phys. Rev. B **99**, 245306 (2019).

[66] B. Royer, A. L. Grimsmo, N. Didier, and A. Blais, Fast and high-fidelity entangling gate through parametrically modulated longitudinal coupling, Quantum **1**, 11 (2017).

[67] S. J. Elman, S. D. Bartlett, and A. C. Doherty, Long-range entanglement for spin qubits via quantum hall edge modes, Phys. Rev. B **96**, 115407 (2017).

[68] A. G. Fowler, Proof of Finite Surface Code Threshold for Matching, Phys. Rev. Lett. **109**, 180502 (2012).

[69] E. Rosenfeld, R. Riedinger, J. Gieseler, M. Schuetz, and M. D. Lukin, Efficient Entanglement of Spin Qubits Mediated by a Hot Mechanical Oscillator, Phys. Rev. Lett. **126**, 250505 (2021).

[70] A. J. Kerman, Quantum information processing using quasiclassical electromagnetic interactions between qubits and electrical resonators, New J. Phys. **15**, 123011 (2013).

[71] M. J. A. Schuetz, B. Vermersch, G. Kirchmair, L. M. K. Vandersypen, J. I. Cirac, M. D. Lukin, and P. Zoller, Quantum simulation and optimization in hot quantum networks, Phys. Rev. B **99**, 241302(R) (2019).

[72] See Supplemental Material at http://link.aps.org/supplemental/10.1103/PhysRevLett.129.066801 for the derivation of the spin-photon coupling strength and of the measurement protocol. We also analyze in detail the two-qubit gate, including a discussion on more general pulse shapes, fidelity, and its dependence on the state of the resonator.

[73] R. Winkler, *Spin–Orbit Coupling Effects in Two-Dimensional Electron and Hole Systems*, edited by G. Höhler, J. H. Kühn, T. Müller, J. Trümper, A. Ruckenstein, P. Wölfle, and F. Steiner, Springer Tracts in Modern Physics (Springer Berlin Heidelberg, Berlin, Heidelberg, 2003), Vol. 191.

[74] F. N. M. Froning, M. J. Rančić, B. Hetényi, S. Bosco, M. K. Rehmann, A. Li, E. P. A. M. Bakkers, F. A. Zwanenburg, D. Loss, D. M. Zumbühl, and F. R. Braakman, Strong spin-orbit interaction and g-factor renormalization of hole spins in Ge/Si nanowire quantum dots, Phys. Rev. Research **3**, 013081 (2021).

[75] C. Kloeffel, M. Trif, P. Stano, and D. Loss, Circuit QED with hole-spin qubits in Ge/Si nanowire quantum dots, Phys. Rev. B **88**, 241405(R) (2013).

[76] S. Bosco and D. Loss, Hole spin qubits in thin curved quantum wells, arXiv:2204.08212.

[77] P. M. Mutter and G. Burkard, Cavity control over heavy-hole spin qubits in inversion-symmetric crystals, Phys. Rev. B **102**, 205412 (2020).

[78] M. Lodari, O. Kong, M. Rendell, A. Tosato, A. Sammak, M. Veldhorst, A. R. Hamilton, and G. Scappucci, Lightly strained germanium quantum wells with hole mobility exceeding one million, Appl. Phys. Lett. **120**, 122104 (2022).

[79] N. Samkharadze, A. Bruno, P. Scarlino, G. Zheng, D. P. DiVincenzo, L. DiCarlo, and L. M. K. Vandersypen, High-Kinetic-Inductance Superconducting Nanowire Resonators for Circuit QED in a Magnetic Field, Phys. Rev. Applied **5**, 044004 (2016).

[80] A. V. Kuhlmann, V. Deshpande, L. C. Camenzind, D. M. Zumbühl, and A. Fuhrer, Ambipolar quantum dots in undoped silicon fin field-effect transistors, Appl. Phys. Lett. **113**, 122107 (2018).

[81] S. Geyer, L. C. Camenzind, L. Czornomaz, V. Deshpande, A. Fuhrer, R. J. Warburton, D. M. Zumbühl, and A. V. Kuhlmann, Self-aligned gates for scalable silicon quantum computing, Appl. Phys. Lett. **118**, 104004 (2021).

[82] A. V. Kuhlmann (to be published).

[83] D. Niepce, J. Burnett, and J. Bylander, High Kinetic Inductance NbN Nanowire Superinductors, Phys. Rev. Applied **11**, 044014 (2019).

[84] L. Grünhaupt, M. Spiecker, D. Gusenkova, N. Maleeva, S. T. Skacel, I. Takmakov, F. Valenti, P. Winkel, H. Rotzinger, W. Wernsdorfer, A. V. Ustinov, and I. M. Pop, Granular aluminium as a superconducting material for high-impedance quantum circuits, Nat. Mater. **18**, 816 (2019).

[85] N. Maleeva, L. Grünhaupt, T. Klein, F. Levy-Bertrand, O. Dupre, M. Calvo, F. Valenti, P. Winkel, F. Friedrich, W. Wernsdorfer, A. V. Ustinov, H. Rotzinger, A. Monfardini, M. V. Fistul, and I. M. Pop, Circuit quantum electrodynamics of granular aluminum resonators, Nat. Commun. **9**, 3889 (2018).

[86] L. Grünhaupt, N. Maleeva, S. T. Skacel, M. Calvo, F. Levy-Bertrand, A. V. Ustinov, H. Rotzinger, A. Monfardini, G. Catelani, and I. M. Pop, Loss Mechanisms and Quasiparticle Dynamics in Superconducting Microwave Resonators Made of Thin-Film Granular Aluminum, Phys. Rev. Lett. **121**, 117001 (2018).

[87] J. J. Viennot, J. Palomo, and T. Kontos, Stamping single wall nanotubes for circuit quantum electrodynamics, Appl. Phys. Lett. **104**, 113108 (2014).

[88] M. Hagmann, Isolated carbon nanotubes as high-impedance transmission lines for microwave through terahertz frequencies, IEEE Trans. Nanotechnol. **4**, 289 (2005).

[89] J. D. Chudow, D. F. Santavicca, and D. E. Prober, Terahertz spectroscopy of individual single-walled carbon nanotubes as a probe of luttinger liquid physics, Nano Lett. **16**, 4909 (2016).

[90] S. Bosco, D. P. DiVincenzo, and D. J. Reilly, Transmission Lines and Metamaterials Based on Quantum Hall Plasmonics, Phys. Rev. Applied **12**, 014030 (2019).

[91] A. Gourmelon, H. Kamata, J.-M. Berroir, G. Fève, B. Plaçais, and E. Bocquillon, Characterization of helical luttinger liquids in microwave stepped-impedance edge resonators, Phys. Rev. Research **2**, 043383 (2020).

[92] Y. Kato, R. C. Myers, D. C. Driscoll, A. C. Gossard, J. Levy, and D. D. Awschalom, Gigahertz electron spin manipulation using voltage-controlled g-tensor modulation, Science **299**, 1201 (2003).

[93] A. Crippa, R. Maurand, L. Bourdet, D. Kotekar-Patil, A. Amisse, X. Jehl, M. Sanquer, R. Laviéville, H. Bohuslavskyi, L. Hutin, S. Barraud, M. Vinet, Y.-M. Niquet, and S. De Franceschi, Electrical Spin Driving by g-Matrix Modulation in Spin-Orbit Qubits, Phys. Rev. Lett. **120**, 137702 (2018).

[94] N. Ares, G. Katsaros, V. N. Golovach, J. J. Zhang, A. Prager, L. I. Glazman, O. G. Schmidt, and S. De Franceschi, SiGe quantum dots for fast hole spin Rabi oscillations, Appl. Phys. Lett. **103**, 263113 (2013).

[95] L. Bellentani, M. Bina, S. Bonen, A. Secchi, A. Bertoni, S. P. Voinigescu, A. Padovani, L. Larcher, and F. Troiani, Toward Hole-Spin Qubits in Si p-MOSFETs within a Planar CMOS Foundry Technology, Phys. Rev. Applied **16**, 054034 (2021).

[96] B. Venitucci, L. Bourdet, D. Pouzada, and Y.-M. Niquet, Electrical manipulation of semiconductor spin qubits within the g-matrix formalism, Phys. Rev. B **98**, 155319 (2018).

[97] B. Hetényi, C. Kloeffel, and D. Loss, Exchange interaction of hole-spin qubits in double quantum dots in highly anisotropic semiconductors, Phys. Rev. Research **2**, 033036 (2020).

[98] T. Fujita, T. A. Baart, C. Reichl, W. Wegscheider, and L. M. K. Vandersypen, Coherent shuttle of electron-spin states, npj Quantum Inf. **3**, 22 (2017).

[99] A. R. Mills, D. M. Zajac, M. J. Gullans, F. J. Schupp, T. M. Hazard, and J. R. Petta, Shuttling a single charge across a one-dimensional array of silicon quantum dots, Nat. Commun. **10**, 1063 (2019).

[100] J. Yoneda, W. Huang, M. Feng, C. H. Yang, K. W. Chan, T. Tanttu, W. Gilbert, R. C. C. Leon, F. E. Hudson, K. M. Itoh, A. Morello, S. D. Bartlett, A. Laucht, A. Saraiva, and A. S. Dzurak, Coherent spin qubit transport in silicon, Nat. Commun. **12**, 4114 (2021).

[101] M. Benito, X. Mi, J. M. Taylor, J. R. Petta, and G. Burkard, Input-output theory for spin-photon coupling in Si double quantum dots, Phys. Rev. B **96**, 235434 (2017).

[102] D. Loss and D. P. DiVincenzo, Quantum computation with quantum dots, Phys. Rev. A **57**, 120 (1998).

[103] Y. Xu, J. Chu, J. Yuan, J. Qiu, Y. Zhou, L. Zhang, X. Tan, Y. Yu, S. Liu, J. Li, F. Yan, and D. Yu, High-Fidelity, High-Scalability Two-Qubit Gate Scheme for Superconducting Qubits, Phys. Rev. Lett. **125**, 240503 (2020).

[104] M. C. Collodo, J. Herrmann, N. Lacroix, C. K. Andersen, A. Remm, S. Lazar, J.-C. Besse, T. Walter, A. Wallraff, and C. Eichler, Implementation of Conditional Phase Gates Based on Tunable zz Interactions, Phys. Rev. Lett. **125**, 240502 (2020).

[105] H. Wang, M. Hofheinz, M. Ansmann, R. C. Bialczak, E. Lucero, M. Neeley, A. D. O'Connell, D. Sank, J. Wenner, A. N. Cleland, and J. M. Martinis, Measurement of the Decay of Fock States in a Superconducting Quantum Circuit, Phys. Rev. Lett. **101**, 240401 (2008).

[106] Y. Makhlin, G. Schön, and A. Shnirman, Dissipative effects in Josephson qubits, Chem. Phys. **296**, 315 (2004).

[107] J. M. Martinis, S. Nam, J. Aumentado, K. M. Lang, and C. Urbina, Decoherence of a superconducting qubit due to bias noise, Phys. Rev. B **67**, 094510 (2003).

[108] L. Cywiński, R. M. Lutchyn, C. P. Nave, and S. Das Sarma, How to enhance dephasing time in superconducting qubits, Phys. Rev. B **77**, 174509 (2008).

[109] J. Yoneda, K. Takeda, T. Otsuka, T. Nakajima, M. R. Delbecq, G. Allison, T. Honda, T. Kodera, S. Oda, Y. Hoshi, N. Usami, K. M. Itoh, and S. Tarucha, A quantum-dot spin qubit with coherence limited by charge noise and fidelity higher than 99.9%, Nat. Nanotechnol. **13**, 102 (2018).